Photodissociation of protonated leucine-enkephalin in the VUV range of 8–40 eV

S. Bari,[1,a)] O. Gonzalez-Magaña,[1] G. Reitsma,[1] J. Werner,[2] S. Schippers,[2] R. Hoekstra,[1] and T. Schlathölter[1]

[1]*KVI Atomic and Molecular Physics, University of Groningen, Zernikelaan 25, 9747AA Groningen, The Netherlands*

[2]*Institut für Atom- und Molekülphysik, Justus-Liebig-Universität, Leihgesterner Weg 217, 35392 Giessen, Germany*

(Received 16 September 2010; accepted 22 October 2010; published online 12 January 2011)

Until now, photodissociation studies on free complex protonated peptides were limited to the UV wavelength range accessible by intense lasers. We have studied photodissociation of gas-phase protonated leucine–enkephalin cations for vacuum ultraviolet (VUV) photons energies ranging from 8 to 40 eV. We report time-of–flight mass spectra of the photofragments and various photofragment-yields as a function of photon energy. For sub-ionization energies our results are in line with existing studies on UV photodissociation of leucine–enkephalin. For photon energies exceeding 10 eV we could identify a new dissociation scheme in which photoabsorption leads to a fast loss of the tyrosine side chain. This loss process leads to the formation of a residual peptide that is remarkably cold internally. © *2011 American Institute of Physics*. [doi:10.1063/1.3515301]

I. INTRODUCTION

Amino acids are the building blocks of peptides and proteins present in all living organisms on Earth. Since amino acids were found in some meteorites[1–3] and are likely to exist in the interstellar medium (ISM),[4,5] transport of prebiotic and biotic molecules from outer space to Earth is considered an alternative to the conventional assumption of purely Earth bound development of life.

Many studies on photo-induced ionization and fragmentation of amino acids have been conducted,[6–8] for instance to be able to recognize signatures of these molecules in the ISM, in comets, and in planetary atmospheres or to understand the mechanisms behind the in–space formation of amino acids. It was already shown that amino acid synthesis from simpler organic molecules can be induced by interaction with cosmic rays,[9,10] spark discharges,[11] ultraviolet (UV)/vacuum ultraviolet (VUV) radiation or simply by thermal excitation.[12,13] Bernstein *et al.*[14] and Caro *et al.*[15] synthesized several amino acids by UV irradiation of interstellar ice grain models and Nuevo *et al.*[16] even concluded that amino acids are always formed when interstellar ice grain models containing C, H, O, and N are irradiated with VUV photons. Even peptide bond formation was observed under VUV irradiation of dry amino acid films or amino acids in icy matrices,[4,17,18] implying that peptides could be formed e.g., on interstellar dust grains or small solar system bodies. An obvious next step now is to investigate the photo stability of peptides. Studies during long duration space missions indicated that dipeptides and the tripeptide tri-L-leucine thioethylester have higher stability upon UV-irradiation than amino acids.[19,20] But how photo stable were the early peptides on Earth and is it possible that intact early peptides have been transported from space to Earth in the gas phase? Van der Gulik *et al.*[21] assume early functional prebiotic peptides to be 3–8 amino acids long. We have therefore chosen the pentapeptide leucine–enkephalin (leu–enk) as an ideal subject for studying peptide response upon photoabsorption. Since photoabsorption cross-section of amino acids typically peak in the VUV range, i.e., at wavelengths shorter than 200 nm,[22] in this study we will focus on VUV-photon absorption. VUV wavelengths are particularly interesting also because in this wavelength range the luminosity of the early Sun was 2 orders of magnitude higher than today so that VUV/UV is assumed to be the most intense radiation on the early Earth during the Hadean period (4.6–3.8 gigayears ago) with no or very dilute atmosphere present.[23]

In the following, we present the first systematic VUV photodissociation study of a free protonated peptide. Leu–enk has the additional advantage that it has already been investigated by a whole arsenal of mass-spectrometric tools. The obtained fragmentation pattern and yields will be interpreted in the context of existing data on leu–enk surface-induced dissociation (SID),[24] blackbody infrared radiative dissociation (BIRD),[25] laser-induced dissociation (LID),[26] multiphoton-induced[27] and collision-induced (CID)[28] mass spectra. The influence of the electronic structure of the peptide and its constituent amino acids on the dissociation and ionization will be discussed.

II. EXPERIMENT

Recently, we have developed a new apparatus (for a sketch, see Fig. 1) in which a home-built electrospray ionization (ESI) source is combined with a radiofrequency (RF) trap and a time-of-flight (TOF) mass spectrometer. This setup has been interfaced with a VUV photon beamline of the third generation synchrotron facility BESSY II in Berlin. Tunable

a)Author to whom correspondence should be addressed. Electronic mail: sadia.bari11@gmail.com.

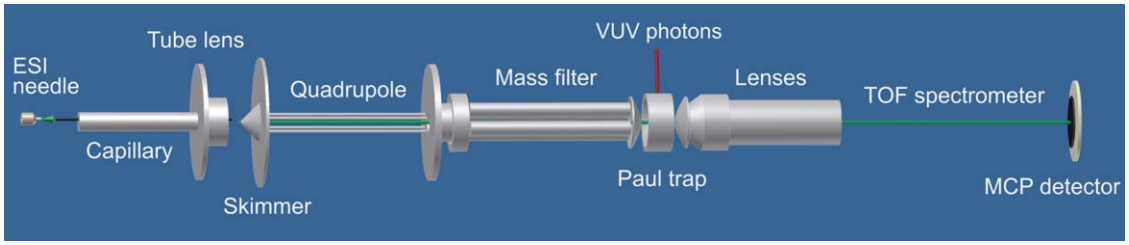

FIG. 1. Experimental setup.

VUV photons in the energy range of 8–40 eV were obtained from the quasi periodic undulator U125/2 (Ref. 29), which consists of 32 dipole magnet periods each 125 mm long, in combination with the 10 m focal length normal incidence monochromator (NIM).[30] In order to achieve maximum photon flux a relatively low resolution of 300 lines/mm grating was employed.

A brief description of the experimental setup follows, which will be described in more detail in a later publication. The singly protonated cations of the pentapeptide (leu–enk, amino acid sequence: YGGFL, $m = 555.62$ amu, a scheme is shown in Fig. 2) were generated in the ESI source from a $\sim$30 μM methanol solution with 1% formic acid. The ions were then passed through a collisionally focusing RF-only quadrupole. After phase space compression, the peptide ions passed an RF-quadrupole mass analyzer. Mass selected protonated leu–enk ions entered a quadrupole ion trap through its endcap (see Fig. 1). The trapped peptides served as a target for the VUV photons.

The base pressure inside the trap chamber was 1×10^{-9} mbar. For collisional cooling of the peptide ions, a He-buffer gas pulse was applied during the trap loading period. The estimated pressure inside the trap increased to 1×10^{-3} mbar, and the trap was typically loaded with protonated peptides over a period of 400 ms. The ion beam was then blocked by means of a 100 V skimmer bias. At the same time the solenoid valve, controlling the He-buffer gas flow, was closed and the pressure in the trap decreased to about 1×10^{-6} mbar.

The VUV photons intersected the Paul trap through the ring electrode. The photon beam focus was chosen to lie in the center of the RF-trap. The geometric beam cross section was 100 μm $\times$ 120 μm (at 25 eV with 20 μm slit width). The

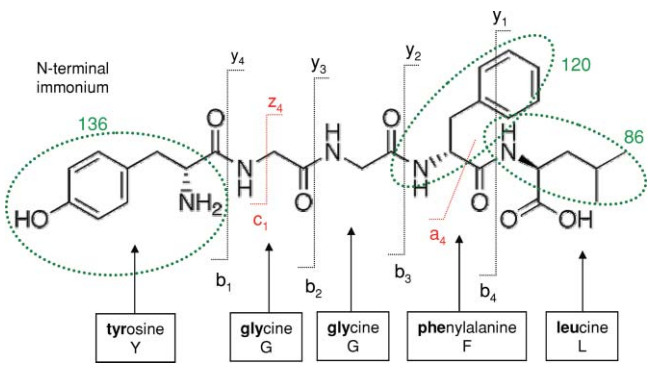

FIG. 2. Structure of leucine–enkephalin with its five constituent amino acids and their three-letter code (bold) and one-letter code indicated. The nomenclature of the fragments as well as the immonium ions are displayed.

photon flux was monitored using a GaAsP–Schottky diode[31] located 23 cm behind the trap center. The protonated peptides were then exposed for about 0.1–1 s to the photon beam which was chopped by a mechanical shutter with a 14 mm aperture. To avoid sizeable contributions of multiple absorption processes, the conditions were chosen such that a total of about 10% of the trapped protonated peptides were dissociated by interactions with photons, i.e., less than approximately 10% of the dissociated peptides underwent absorption of more than one photon. After 80 ms of irradiation the trapped protonated peptides and their cationic dissociation products were extracted into a linear TOF mass spectrometer ($M/\Delta M = 200$) by applying a bias voltage ($U_{bias} = \pm$ 200 V, duration: 5 μs) to the RF-trap endcaps. The ions were detected by a microchannel-plate detector with the front plate biased to –2 kV and the anode kept at ground potential. The detector signal was recorded by a 1 GHz digitizer.

Despite the low background pressure and a liquid nitrogen cooled cryo-trap close to the RF-trap, contamination of the buffer gas or neutral molecules from the ESI source may have contributed to the mass spectra. To extract the mass spectrum due to leu–enk fragmentation only, the data acquisition was divided into successive cycles of three mass scans. In each cycle, first the TOF spectrum resulting from VUV photon irradiation of the trapped protonated peptides and neutral residual gas was recorded (inclusive scan). To obtain the net effect of photon irradiation upon the trapped protonated peptides, in a second scan the photon beam was blocked and a TOF spectrum of the initial trap content only was recorded. For the third scan, the ESI source was switched off and the TOF spectrum resulting from the photoionization of residual gas molecules was recorded. The latter two spectra were then subtracted from the inclusive scan. A three-scan cycle took about 3 up to 6 s. To obtain the final mass spectra a series of 2000–6000 cycles was accumulated for each photon energy.

In order to be able to directly compare peak intensities and integrals from mass spectra obtained at different photon energies, it was necessary to normalize the mass spectra. The relative photon flux was determined from the photocurrent of the GaAs photodiode, divided by its photonenergy dependent quantum efficiency. Note, that the photodiode had not recently been calibrated and accordingly no very reliable numbers for the absolute flux could be obtained. The density of the leu–enk cation target was determined from the integral of the unirradiated leu–enk peak in the TOF spectrum. Trap depth and RF-frequency were not changed during the experimental campaign, i.e., the target volume was constant. Typically ion-clouds trapped in RF-traps at the parameters used in our study were about 1 mm in diameter. The exact target volume

is difficult to determine. However, with relative photon flux, relative target density and irradiation time known, the spectra could be normalized and peak integrals from the mass spectra could be interpreted as relative photodissociation cross-sections.

III. RESULTS

Typical normalized fragment cation mass spectra obtained after irradiation of leu–enk with 8, 15, and 20 eV photons are shown in Fig. 3. Note that the intensity range is about a factor of 15 smaller for the 8 eV spectrum as compared to the 15 and 20 eV spectra. Particularly the spectra at 15 and 20 eV exhibit some resemblance to our recent keV ion-induced dissociation (KID) results.[32]

In general in the photon energy range 10–40 eV, the spectra are dominated by fragments with $m/q = 80$–240 amu. The immonium ions at 86 (L), 120 (F), 136 (Y), and the common fragments of these groups (91 and 107) are strongly contributing. For the photon energy range 10–40 eV the VUV induced fragmentation spectra differ strongly from what is observed in CID (Ref. 28), SID (Ref. 24) and also IR multiphoton absorption[27] where fragments with m/q exceeding 350 dominate the spectra and immonium fragments are usually weak.

In the following paragraphs the spectra obtained at the photon energies ($h\nu$) 8, 15, and 20 eV will be described in more detail.

A. 8 eV: Below ionization threshold

If the photon energy falls short of the ionization energy (IE), photoabsorption transfers the protonated peptide into an electronically excited state. We have used density functional theory (DFT) calculations (B3LYP level, 6-31+G(d,p) basis set) using GAUSSIAN 03 (Ref. 33) to determine an IE = 8.87 eV for the lowest energy conformer of protonated leu–enk determined by IR spectroscopy and quantum chemical calculations.[34]

The fragmentation patterns of leu–enk obtained with 8 and 9 eV [Fig. 3(a)] photons are very different from the spectra for all the other photon energies, most probably because at these low photon energies the leu–enk cation cannot be directly photoionized. The peak at $m/q = 278/279$ assigned to b_3/y_2 (possibly with a small contribution of the $(M+H)^{2+}$ radical dication) is the strongest peak followed by the immonium ion with $m/q = 120$ (F). The fragments $a_4 = 397$ and $b_4 = 425$ which are most abundant when dissociation techniques such as CID and BIRD (Ref. 25) are used are either weak (a_4) or absent (b_4).

The peaks with mass-to-charge ratios of 380 (a_4-NH_3), 323 (380-glycine residue), 233 (380-phenylalanine residue), 217 (380-tyrosine residue), 262 (GGF), 205 (GF), and 177 (GF–CO) are due to internal fragments. Probably these fragments result from a cyclic rearrangement of the a_4 intermediate as identified by Vachet *et al.*[35] for CID of leu–enk investigated by multiple stage mass analysis in a quadrupole ion trap. At higher photon energies, all these fragments with the exception of GF are suppressed.

The peaks at $m/q = 449$ and 465, corresponding to tyrosine side chain loss (107) and phenylalanine side chain loss (91) respectively, are clearly visible for 8 eV photon energy. These peaks are also observed by Tabarin and co-workers,[26] who employed LID at photon energies between 4.4 eV (280 nm) and 5.6 eV (220 nm) but are usually not present in CID spectra.

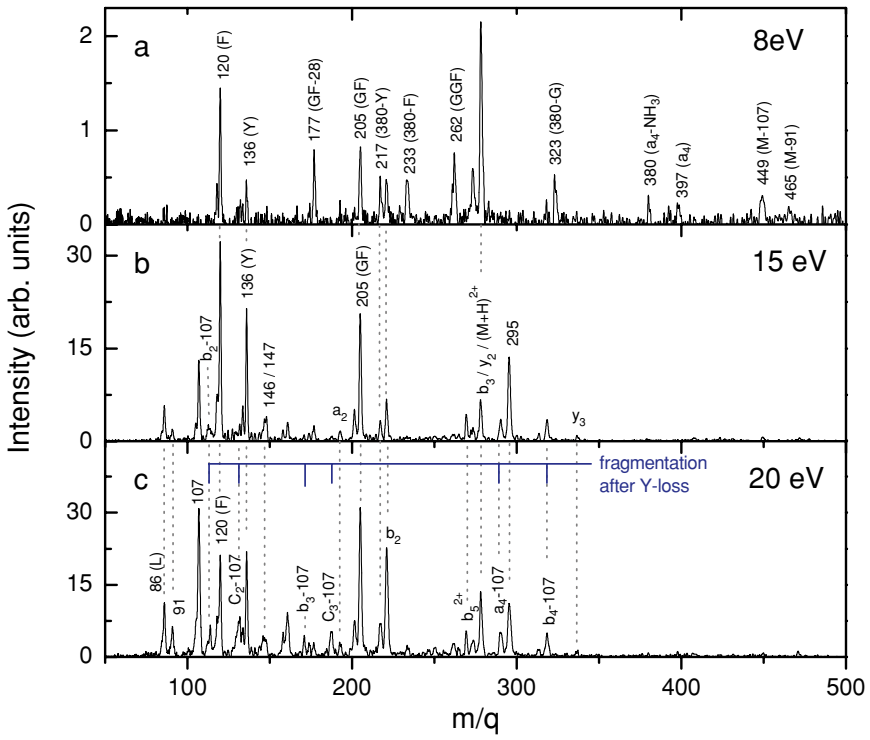

FIG. 3. VUV photon-induced mass spectra of protonated leu–enk at 8, 15, and 20 eV photon energy.

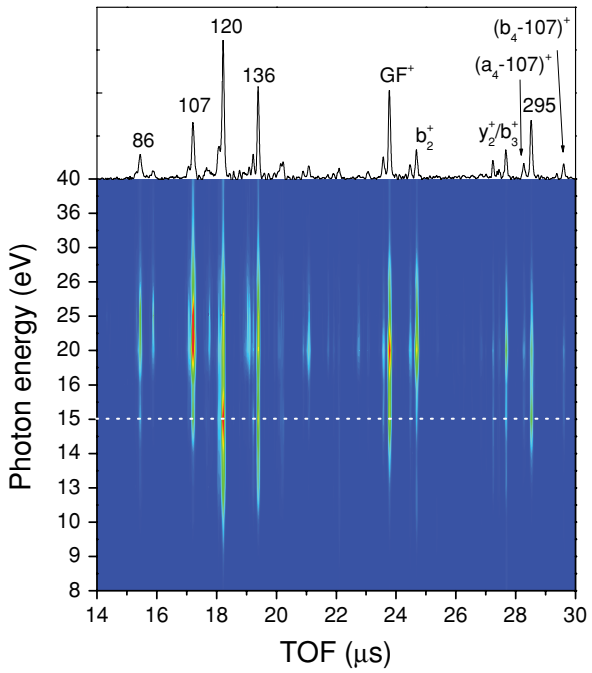

FIG. 4. Contour plot of photofragment time-of-flight versus photon energy. All photon energies for which spectra were acquired are given on the *y* axis. The spectrum on top represents a cut through the contour plot indicated by the white dotted line at 15 eV [identical with the spectrum shown Fig. 3(b)].

B. 15 and 20 eV: Above ionization threshold

Dramatic changes in the spectrum are observed when photon energies are exceeding 9 eV. The main fragments at 15 eV [see Fig. 3(b)] are the immonium ions with $m/q = 120$ (F) and $m/q = 136$ (Y) and the internal fragment with $m/q = 205$ (GF). The peak at $m/q = 295$ represents another step in the decay of the cyclic rearranged a_4, which underwent NH_3 loss forming a fragment with $m/q = 380$ followed by glycine loss resulting in an even smaller fragment with $m/q = 323$ from which it is formed by CO loss.[35] Note that the $m/q = 295$ fragment is absent in the 8 and 9 eV spectra. Compared to $h\nu = 15$ eV the mass spectrum appears richer at 20 eV photon energy [see Fig. 3(c)], i.e., a number of low intensity peaks are getting stronger. The Y side chain fragment at $m/q = 107$ becomes the strongest peak in the spectrum and in general immonium ions and related fragment ions of tyrosine, phenylalanine, and leucine are strong in the 20 eV spectrum. Also, a relatively strong $b_2 = 221$ peak is observed. An interesting feature of Fig. 3(c) is a series of *a*, *b*, and *c* fragments which have lost the tyrosine side chain.

C. Fragment yields

An overview of the normalized leu–enk photodissociation TOF-spectra covering the whole range of photon energies between 8 and 40 eV is displayed as a color-coded contour plot in Fig. 4. The photon energies at which spectra were acquired are given on the *y* axis. The dotted white line in the contour plot at 15 eV indicates the cut through the data, which is represented by the TOF spectrum displayed on top [identical with Fig. 3(b)]. The data in between measured photon energies have been obtained by mere interpolation. Note the nonlinear photon energy scale! It is obvious from Fig. 4 that all fragment peaks exhibit a strong photon-energy dependence. As mentioned before, at $h\nu = 8$ eV the relative fragment yields are weak and fragments reach their peak intensities between 10 and 30 eV. For photon energies exceeding 30 eV, the relative yields are decreasing again. Different fragments apparently peak at different photon energies. For instance, $m/q = 120$ (F) peaks at 15 eV whereas $m/q = 107$ (tyrosine side chain) peaks at 20–25 eV.

For a number of stronger fragments, photofragment yield curves are displayed in Fig. 5. The statistical uncertainties, originating from the statistics and data handling, are very small and mostly not even visible in the plots. Further systematic error sources, such as deviations from the calibration of the photodiode and contamination from higher harmonics from the undulator during irradiation at lower energies are not taken into account. All yields exhibit a broad peak which in most cases has a full width at half maximum of about 10 eV. Only for $m/q = 120$ (F) there is an absolute maximum at $h\nu = 15$ eV whereas the maximum is around $h\nu = 20$ eV for the remaining fragments. In addition, there might be a local maximum at $h\nu = 15$ eV photon energy for many fragment ions. The tyrosine side chain fragment ($m/q = 107$), the F-immonium ion and the internal fragment GF reach highest yields amongst the fragments.

Rather than by summation of all photofragment ion yields, the total photodissociation yield can be obtained by subtraction of the parent $(M+H)^+$ peak after irradition from the parent peak prior to the irradiation. Figure 6 shows the normalized total photodissociation yield as a function of the photon energy. Again, the yield curve features a broad peak with a local maximum at about 15 eV and a total maximum at about 20 eV. Note, that due to a *m/q* dependence of the detection efficiency and due to multiplicity into two or more fragments, the total photodissociation yield is smaller than the sum of the fragment yields.

IV. DISCUSSION

In the photon energy range under study here (8–40 eV), two different regimes of photoabsorption triggered dissociation processes have to be considered.

(I) For $h\nu <$ IE vertical ionization is ruled out and mainly *excitation* processes contribute. (Note, that adiabatic channels such as ion-pair formation might also lead to photoion production below the vertical ionization threshold.) The dominating processes here are valence transitions. (To a smaller extent, resonant excitation into Rydberg orbitals can take place.) Three groups of chromophores contribute to valence transitions in peptides, namely the peptide bond itself, the aromatic side chains, and the terminal amine and carboxyl groups. However, it is the peptide bond that is expected to contribute dominantly in the 8–9 eV photon-energy range studied here.[36] The peptide bond can be viewed as a four level system consisting of two doubly occupied π-orbitals (π_1 and π_2), the O lone pair and an antibonding empty $\pi^\star$ orbital with the π_1–$\pi^\star$ transition being responsible for the absorption around $h\nu = 9$ eV. At 8 eV, so-called charge transfer

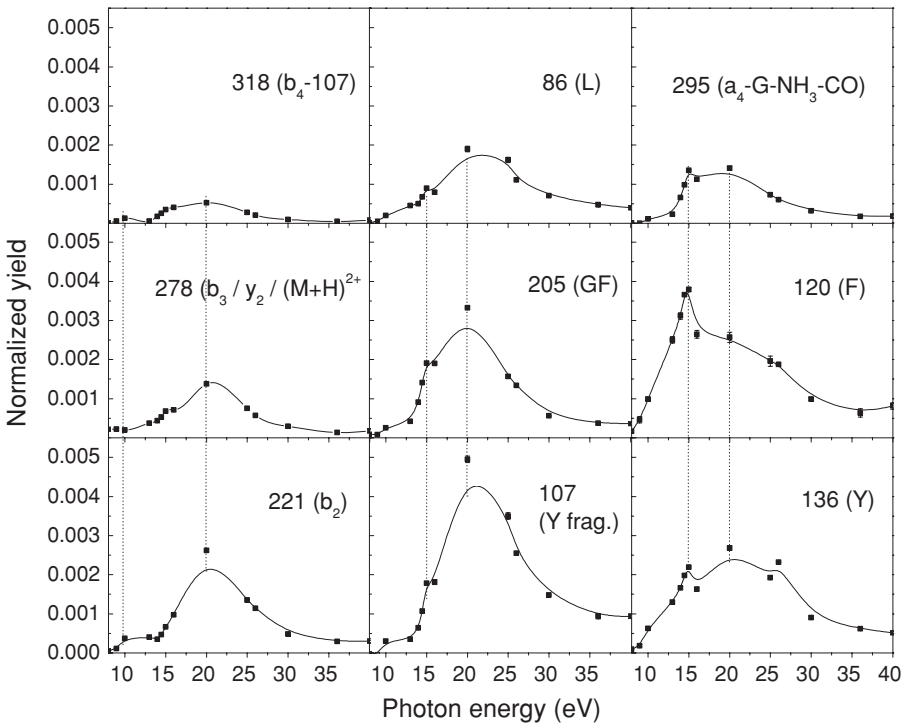

FIG. 5. Protonated leu–enk photofragment ion yields as a function of photon energy for nine important fragments. All spectra have identical scales.

transitions of a π_2 electron from one peptide bond into the $\pi^\star$ orbital of an adjacent peptide bond can still contribute.[37]

The initial photoexcitation processes can be followed by radiative de-excitation, intramolecular vibrational redistribution (IVR), direct dissociation through dissociative electronic states, and other processes, which can differ greatly in timescales involved. When we assume that the excitation of one of the peptide bonds is followed by IVR, we can directly compare our results to the SID studies by Laskin.[24] For 50 eV protonated leu–enk collisions with a self-assembled alkane thiolate monolayer, a maximum of about 17% of the collision energy is transferred into the peptide[38] implying about 8.5 eV of internal energy—about the same as deposited by 8 or 9 eV photoexciation here. The SID spectrum, qualitatively similar to our photoexcitation data [see Fig. 3(a)], is dominated by 120 (F), 136 (Y), b_3/y_2, a_4, and a_4-NH_3. Internal fragments GF-28, GF, GGF, and FYG are observed as well. Laskin[24] found a strong time dependence of a_4-NH_3 and FYG and concludes that these fragments are associated with the cyclic rearrangements previously mentioned. This cyclic a_4 rearrangement has already been invoked earlier by Vachet and co-workers.[35] The fragments b_3, GF, and 120 (F) show no time dependence and are formed following entropically favored pathways.[24]

Despite the good agreement in fragments observed, the fragment yields are very different: For SID, $a_4 = 397$ and $b_4 = 425$ are the strongest fragments whereas (F) and (Y) are weak. The opposite is true for our 8 eV photon data [Fig. 3(a)]. The reason for the difference could lie in the possibility of dissociation through repulsive electronic states occurring before IVR: At $h\nu = 8$ eV, we observe the relatively strongest contribution of $m/q = 449$ and $m/q = 465$ due to loss of the neutral Y-side chain and the neutral F-side chain, respectively. Tabarin *et al.*[26] observed identical loss processes for photon energies between 4.4 and 5.6 eV after photoabsorption in either of the tyrosine and phenylalanine chromophores. This was already earlier interpreted as an indication of fast dissociation occurring before internal vibrational redistribution (IVR).[39] For our data this implies that sizeable absorption in the tyrosine and phenylalanine chromophores still takes place for photon energies of 8 or 9 eV.

(II) For $h\nu >$ IE the protonated peptide can be *photoionized* and a protonated leu–enk dication radical is formed. (The process in which a stronger bound electron can get photoexcited below the ionization threshold will not be considered

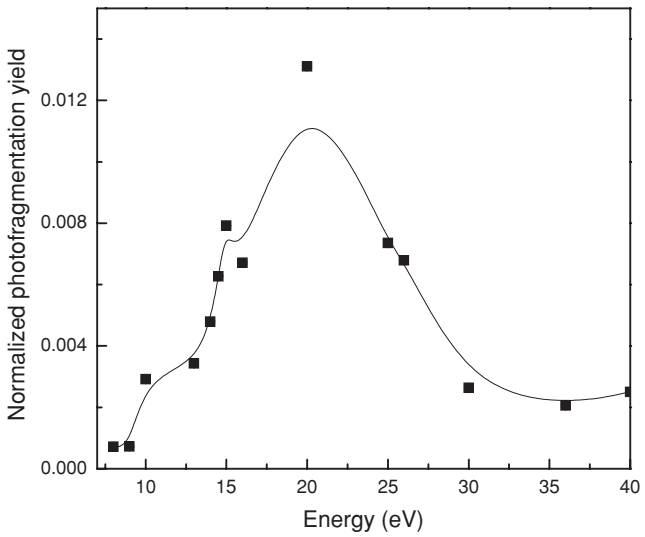

FIG. 6. Total photodissociation yield of protonated leu–enk as a function of photon energy (defined as the photon-induced depletion of the parent ion signal).

because the subsequent dissociation dynamics probably resembles what was discussed for the (I) case and relatively small fragment yields are expected due to the higher excitation energies.)

Hence, when the photon energy passes the IE, a fundamentally different regime is reached. Instead of the hot singly charged system discussed in (I), an electron from a (local) highest occupied molecular orbital (HOMO) is photoionized and a comparably cold doubly charged system is formed. The close to threshold regime, has been explored, e.g., by Walter *et al.*[40] In their experiments resonant two-photon absorption by neutral laser-desorbed smaller peptides only led to negligible fragmentation.

When the photon energy continues to increase, electrons from deeper lying molecular orbitals become accessible for ionization. This gives rise to the formation of an intermediate $(\text{leu–enk} + \text{H})^{2+}$ complex in an electronically excited state. If IVR dominates, the excess energy $E_{\text{int}} \approx h\nu$-IE remains in the $(\text{leu–enk} + \text{H})^{2+}$ complex. How much excitation energy is needed to induce fragmentation of this intermediate system? Laskin showed that in protonated leu–enk typical fragmentation pathways leading, e.g., to GF formation open up for internal energies between 3 and 4 eV, if reaction times of the order of a second are employed. These reaction times are comparable to the ones used in the present study and our results can thus be explained within this framework:

For most fragments (except the $m/q = 120$ (Y) and the $m/q = 136$ (Y) immonium ions which will be discussed later) the yield is only increasing very weakly up to $h\nu = 13$ eV from where it starts to increase sharply [see Fig. (5)]. Apparently here the internal energy overcomes the thresholds for dissociation following IVR. Most fragments display a local maximum at $h\nu = 15$ eV as well as a broader and more intense maximum around $h\nu = 20$ eV. It is known that the photoabsorption cross sections of larger peptides agree quite well with the absorption cross sections of the isolated amino acids, i.e., that photoabsorption remains a local process.[41] It is thus instructive to compare our data with photofragment yield curves measured by Jochims *et al.*[7] for neutral gas phase amino acids. Their photofragment curves e.g., for glycine exhibit inflections at each energy where a deeper lying molecular orbital becomes accessible (see also Ref. 42) and are qualitatively similar to our results. The photofragment yield curves thus depend on the energetic ordering of the valence molecular orbitals, i.e., the molecular density of states. It is useful to look into the photoelectron emission spectra from the four amino acids present in leu–enk to get a deeper insight into the origin of the fragment-yield curves presented in Fig. 5.

For glycine, the photoelectron emission spectrum obtained at 99 eV (Ref. 43) is dominated by intense peaks due to valence electrons at binding energies between 10 and 19 eV, with the lowest three being due to the N lone pair n_N (HOMO), the hydroxyl O lone pair n_O and the bonding carbonyl orbital π_{CO}. The weaker peaks at higher binding energies are due to single electron ionizations. The same ordering is observed also for other aliphatic amino acids so we expect similar highest occupied molecular orbitals for leucine as well.

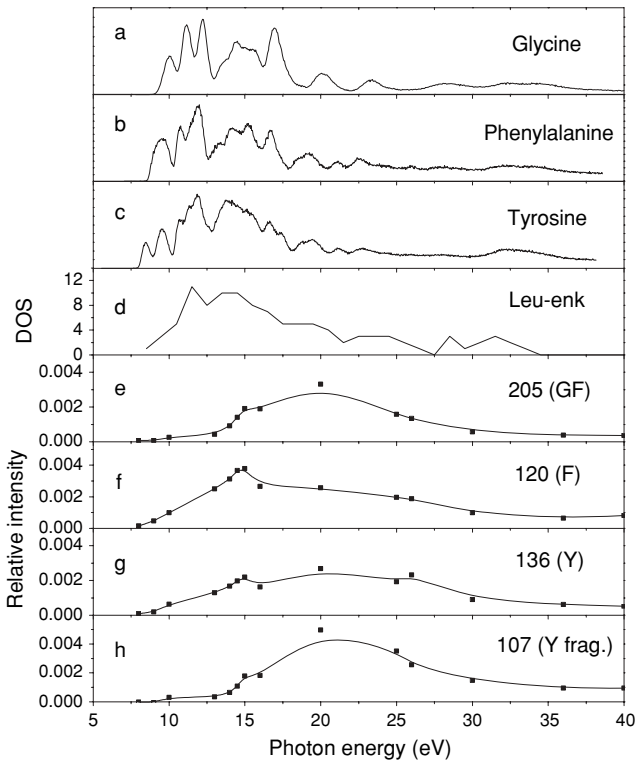

FIG. 7. Comparison of the photoelectron data for the amino acids glycine (Ref. 43) (a), phenylalanine (Ref. 44) (b), and tyrosine (Ref. 43) (c) with the calculated molecular valence orbital density of leu–enk (d) and the fragment yields of GF (e), F (f), Y (g) and the 107 fragment of Y (h).

The aromatic amino acids tyrosine and phenylalanine have a slightly different valence structure since the π orbitals on the phenyl (phenylalanine) and phenol (tyrosine) rings have lower ionization energies than the n_N orbitals. For phenylalanine, the phenyl π_1 and π_2 orbitals and the n_N lone pair coincide energetically at 9.5 eV whereas for tyrosine, the π_1 peak is located at 8.5 eV whereas π_2 and n_N are found at 9.6 eV. For both amino acids, the intense peaks originating from valence electrons span a binding energy range up to about 18 eV,[44] i.e., the amino acid valence spectra qualitatively agree in the width of the peaks with the fragment yields measured here.

In the DFT calculations mentioned before, we have calculated the density of molecular valence orbitals for protonated leu–enk [see Fig. 7(d)]. The above mentioned photoelectron data[43,44] for the different amino acids are displayed for comparison [see Figs. 7(a)– 7(c)]. Clearly the peptide electronic structure overall resembles those of the amino acids. The three highest occupied molecular orbitals for protonated leu–enk are located on the phenyl ring (HOMO, HOMO-1) and on the phenol ring (HOMO-2). Even though the ordering deviates from the case of the isolated neutral amino acids, we find agreement in the sense that the aromatic side chains host the most weakly bound electrons. As mentioned above, in the context of dissociation following IVR, states with binding energies of about 13 eV and more are relevant, since only ionization from these states leads to dissociation. Figure 7(e) displays the GF yield (a typical fragment formed after IVR) for comparison with the protonated leu–enk density of states.

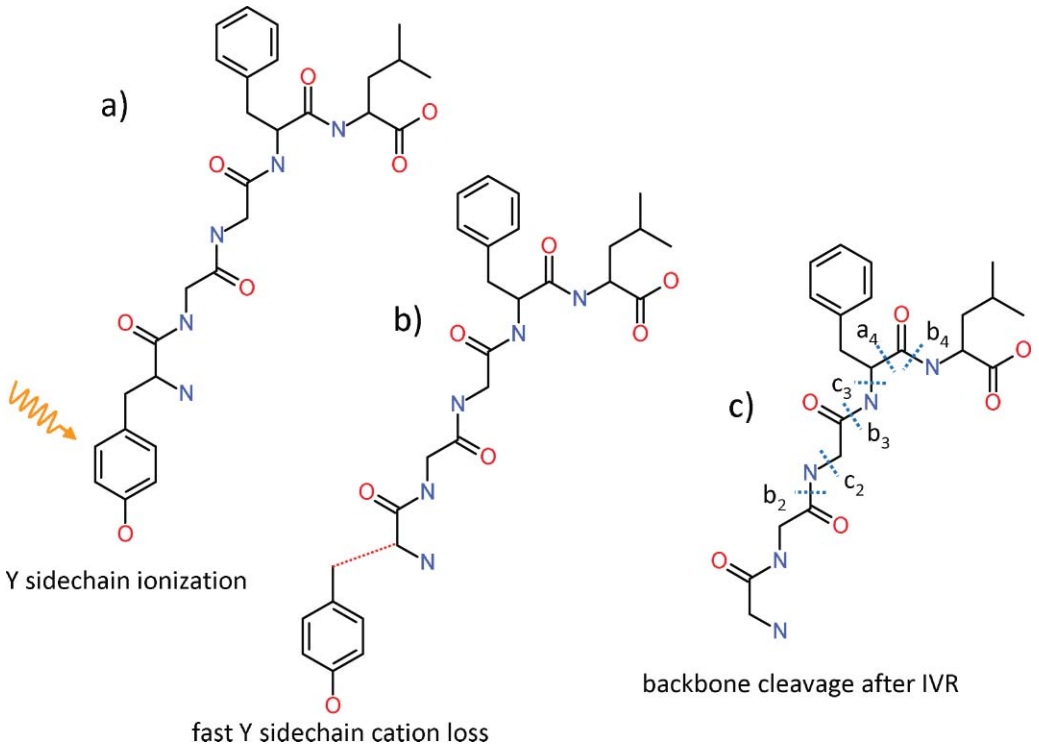

FIG. 8. The three step process of leu–enk dissociation. After ionization (a) the peptide looses the Y fragment (107) nonergodic (b) and the remaining peptide breaks at the backbone following IVR (c).

It is obvious that the rise of the fragment yield coincides with the second maximum of the density of states, where about 20 molecular orbitals are found between 13 and 15 eV. The further increase of the fragment yield up to photon energies of about 20 eV can be explained with the fact that up to this energy additional molecular orbitals become available for photoionzation, i.e., the absorption cross section is expected to increase. Only a couple of states lie deeper than 20 eV and these are almost exclusively atomic 2s orbitals with small cross sections. Accordingly, the fragment yield decreases above 20 eV.

From Figs. 4, 7(f), and 7(g) it is obvious that above 9 eV (only) the $m/q = 120$ (F) and the $m/q = 136$ (Y) immonium ions are strongly increasing, i.e., these fragments are not formed following simple IVR. The yields of both immonium ions peak at $h\nu \approx 15$ eV which for (F) even is the absolute maximum in yield. The π orbitals from the aromatic side chains have low binding energies up to around 12 eV so a large fraction of the ionization processes in this photon energy range will certainly originate from the aromatic groups. Probably in these cases fast dissociation via repulsive molecular states is more efficient than dissociation following IVR.

The most remarkable feature in particular well above the ionization threshold is the fact that $m/q = 107$ (the tyrosine side chain) shows up and becomes the strongest peak [Figs. 4 and 7(h)]. Note that to our knowledge for leu–enk this fragment ion has been only observed before in our previous KID studies.[32] But this fragment ion also is the dominant peak in dissociative photoionization of neutral gas phase tyrosine.[43,44] Loss of a charged aromatic side chain, i.e., breaking of the C_α–C_β bond for a neutral tryptophan–gly$_n$ peptide has also been observed.[45] Below the ionization threshold we infer loss of the neutral $m/q = 107$ tyrosine side chain (and of the $m/q = 91$ phenylalanine side chain) from the observed peak M-107 at $m/q = 449$ (and M-91 at $m/q = 465$). Above threshold, the additional charge gives rise to a charge separation process. Also in this case, the process underlying the dissociation cannot be IVR but probably involves a repulsive molecular state.

Together with the 107 fragment ion, a number of N-terminal fragments are observed, which are due to backbone scission accompanied by the loss of the (N-terminal) tyr-side chain, namely $(b_2 - 107)^+$, $(c_2 - 107)^+$, $(b_3 - 107)^+$, $(c_3 - 107)^+$, $(a_4 - 107)^+$, and $(b_4 - 107)^+$. In high energy CID studies, usually only side chain loss of the amino acid at which the backbone cleavage occurred is observed. Moreover, even in such cases loss or fragmentation of aromatic side chains is typically weak or even absent.[46] In our KID study on protonated leu–enk on the other hand, we have observed similar dissociation dynamics.[32]

In case of photoionization the electron is removed from one of the HOMOs located on the tyr- and phe- side chains which apparently induces nonergodic fragmentation similar to the LID case, i.e., fast scission of the Y C_α–C_β bond. Since during photoionization the electron is not excited but removed, the side chain is positively charged and appears as the dominant feature in the mass spectrum [Fig. 3(c)]. Note that Tabarin *et al.* accordingly did not observe this fragment ion in their LID spectra.[26] The remaining protonated peptide cation then undergoes IVR before the excess excitation energy induces backbone scission according to the mobile proton model:[47] Upon an increase of vibrational excitation energy, the proton attached to the remaining

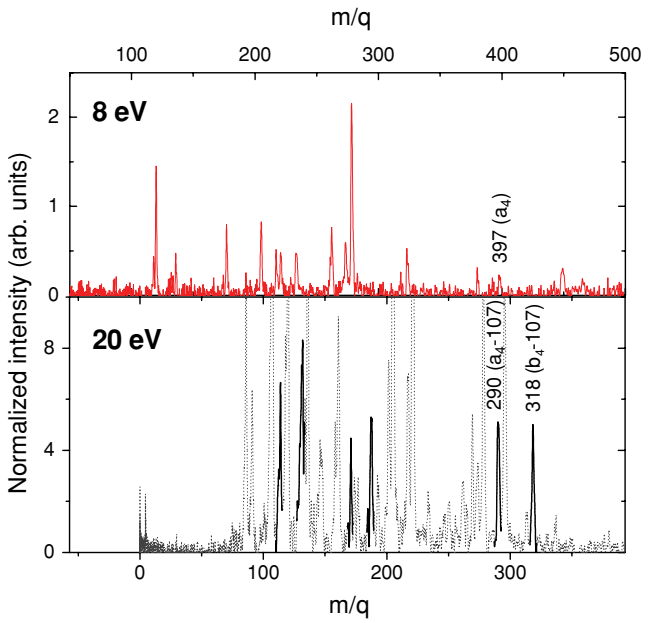

FIG. 9. Comparison of the photofragmentation spectra at 8 eV (top) and at 20 eV (bottom). The 20 eV spectrum was shifted by $m/q = 107$ and the peaks due to tyrosine side chain loss were highlighted.

peptide becomes mobile and samples various protonation sites within the molecule. This way, a fragmentation pattern as expected for CID but shifted to lower masses by 107 amu arises. Figure 8 visualizes the discussed sequence of processes.

This observation has interesting implications in the astrobiological context mentioned in the introduction. Figure 9 again displays the mass spectrum obtained for photoexcitation with 8 eV photons as well as the highlighted part of the 20 eV spectrum, that is due to $m/q = 107$ cation loss. For a better comparison, the latter spectrum has been shifted in m/q by 107. The most obvious finding is that for the 20 eV spectrum relatively more intense peaks are found at larger m/q. In particular in the $m/q = 107$ cation loss case, the a_4 and b_4 fragments are very strong. The ratio of these peaks can be used to compare internal energies of the respective system before fragmentation occurred. Laskin[24] showed for instance that in SID a_4 can be formed above 20 eV collision energy with a maximum at 45 eV. b_4 on the other hand can be formed above 10 eV and peaks at 35 eV. At photon energies of 8 or 9 eV (corresponding to 50 eV or more of collision energy in SID), we observe no b_4 fragment cations. For the case of $m/q = 107$ cation loss, equal a_4 and b_4 yields are observed, implying ~4.8 eV of internal energy.

The fast loss of the charged tyrosine side chain after 20 eV photoabsorption is thus an efficient mechanism to cool the remaining peptide. It is conceivable, that such loss processes facilitate survival of functional peptide substructures after absorption of very energetic photons.

V. CONCLUSION

We have shown that in the photon energy range 8–40 eV different regimes of dissociation processes, below and above IE, have to be considered. Below the ionization energy the photon energy (8–9 eV) is mainly absorbed by the peptide bonds which leads to slow fragmentation governed by IVR. Furthermore we explain differences in qualitatively similar SID spectra in this regime by the possibility of fast dissociation through repulsive states before IVR after absorption of the tyr- and phe- side chain chromophores.

Most fragment yields have a local maximum at a photon energy of 15 eV as well as an absolute broad maximum at 20 eV. This shape can be explained qualitatively by comparison with photoemission spectra of the constituent amino acids and the leu–enk density of molecular states.

At photon energies higher than the ionization energy the relative cross sections of most fragments show a substantial increase above $h\nu = 13$ eV where the internal energy of the intermediate ionized leu–enk overcomes the dissociation threshold following IVR. An exception are the immonium fragments F and Y where fast dissociation through repulsive states competes with IVR at lower energies.

The tyrosine side chain fragment at $m/q = 107$ shows up at ionization threshold and becomes the strongest peak. This fragment was the first time for leu–enk observed in our KID (Ref. 32) studies. Also here, the electron from the HOMO located on the tyrosine side chain is removed inducing fast fragmentation of the C_α–C_β bond leading to a charged fragment.

With the loss of the tyrosine side chain fragment a number of N-terminal fragments are observed accompanied with the loss of the tyrosine side chain. From the ratio of the related a_4/b_4 fragments we could deduce the internal energy and concluded that the fast nonergodic 107 fragment ion loss efficiently cools the residual peptide.

This efficient cooling process seems to allow for survival of early functional peptide substructures under very energetic photon irradiation. Therefore, it is conceivable that substructures of peptides could survive on the early Earth and also transportation to it, providing a basis for the formation of new peptides.

ACKNOWLEDGMENTS

The research leading to these results has received funding from the European Community's Seventh Framework Programme (FP7/2007–2013) under Grant agreement No. 226716. J.W. and S.S. gratefully acknowledge financial support by the Helmholtz Center Berlin. The authors are deeply grateful for the beam line support from Gerd Reichardt.

[1] J. Cronin and S. Chang, *Chemistry of Life's Origin* (Kluwer Academic, Dordrecht 1993), Vol. 416, pp. 209–258.
[2] J. Cronin and S. Pizzarello, Science **275**, 951 (1997).
[3] P. Ehrenfreund, D. Glavin, O. Botta, G. Cooper, and J. Bada, Proc. Natl. Acad. Sci. U. S. A. **98**, 2138 (2001).
[4] N. B. Gontareva, E. A. Kuzicheva, and V. N. Shelegedin, Planet Space Sci. **57**, 441 (2009).
[5] M. Maurette, Origins Life Evol. Biosphere **28**, 385 (1998).
[6] M. Schwell, F. Dulieu, and S. Leach, VUV response of prebiotic and biotic molecules, in *Exo-/Astro-Biology*, volume 496 of *ESA special publication*, pp. 133–136, ESA publications division c/o ESTEC, 2001.
[7] H. Jochims, M. Schwell, J. Chotin, M. Clemino, F. Dulieu, H. Baumgärtel, and S. Leach, Chem. Phys. **298**, 279 (2004).

[8]M. Schwell, H.-W. Jochims, H. Baumgärtel, F. Dulieu, and S. Leach, Planet. Space Sci. **54**, 1073 (2006).
[9]K. Kobayashi, T. Kasamatsu, T. Kaneko, J. Koike, T. Oshima, T. Saito, T. Yamamoto, and H. Yanagawa, Adv. Space Res. **16**, 21 (1995).
[10]K. Kobayashi, T. Kaneko, T. Saito, and T. Oshima, Origins Life Evol. Biosphere **28**, 155 (1998).
[11]S. Miller, Science **117**, 528 (1953).
[12]K. Harada and S. Fox, Nature (London) **201**, 335 (1964).
[13]B. Simoneit, Adv. Space Res. **33**, 88 (2004).
[14]M. Bernstein, J. Dworkin, S. Sandford, G. Cooper, and L. Allamandola, Nature (London) **416**, 401 (2002).
[15]G. Caro, U. Meierhenrich, W. Schutte, B. Barbier, A. Segovia, H. Rosenbauer, W. Thiemann, A. Brack, and J. Greenberg, Nature (London) **416**, 403 (2002).
[16]M. Nuevo, G. Auger, D. Blanot, and L. d'Hendecourt, Origins Life Evol. Biosphere **38**, 37 (2008).
[17]E. Kuzicheva and N. Gontareva, J. Evol. Biochem. Physiol. **37**, 515 (2001).
[18]F. Kaneko, M. Tanaka, S. Narita, T. Kitada, T. Matsui, K. Nakagawa, A. Agui, K. Fujii, and A. Yokoya, J. Electron Spectrosc. Relat. Phenom. **144**, 291 (2005).
[19]B. Barbier, A. Chabin, D. Chaput, and A. Brack, Planet Space Sci. **46**, 391 (1998).
[20]F. Boillot, A. Chabin, C. Bure, M. Venet, A. Belsky, M. Bertrand-Urbaniak, A. Delmas, A. Brack, and B. Barbier, Origins Life Evol. Biosphere **32**, 359 (2002).
[21]P. van der Gulik, S. Massar, D. Gilis, H. Buhrman, and M. Rooman, J. Theor. Biol. **261**, 531 (2009).
[22]T. Inagaki, Biopolymers **12**, 1353 (1973).
[23]C. Chyba and C. Sagan, Nature (London) **355**, 125 (1992).
[24]J. Laskin, J. Phys. Chem. A **110**, 8554 (2006).
[25]P. Schnier, W. Price, E. Strittmatter, and E. Williams, J. Am. Soc. Mass Spectrom. **8**, 771 (1997).
[26]T. Tabarin, R. Antoine, M. Broyer, and P. Dugourd, Rapid Commun. Mass Spectrom. **19**, 2883 (2005).
[27]R. Jockusch, K. Paech, and E. Williams, J. Phys. Chem. A **104**, 3188 (2000).
[28]V. Rakov, O. Borisov, and C. Whitehouse, J. Am. Soc. Mass Spectrom. **15**, 1794 (2004).
[29]J. Bahrdt, W. Frentrup, A. Gaupp, M. Scheer, W. Gudat, G. Ingold, and S. Sasaki, Nucl. Instrum. Methods Phys. Res. A **467**, 130 (2001).
[30]G. Reichardt, J. Bahrdt, J. Schmidt, W. Gudat, A. Ehresmann, R. Müller-Albrecht, H. Molter, H. Schmoranzer, M. Martins, N. Schwentner, and S. Sasaki, Nucl. Instrum. Methods Phys. Res. A **467**, 462 (2001).
[31]M. Krumrey, E. Tegeler, J. Barth, M. Krisch, F. Schäfers, and R. Wolf, Appl. Optics **27**, 4336 (1988).
[32]S. Bari, R. Hoekstra, and T. Schlathölter, Phys. Chem. Chem. Phys. **12**, 3376 (2010).
[33]M. J. Frisch, G. W. Trucks, H. B. Schlegel *et al.*, Gaussian 03, Revision C.02 (Gaussian, Inc., Wallingford, CT, 2004).
[34]N. C. Polfer, J. Oomens, S. Suhai, and B. Paizs, J. Am. Chem. Soc. **129**, 5887 (2007).
[35]R. Vachet, B. Bishop, B. Erickson, and G. Glish, J. Am. Chem. Soc. **119**, 5481 (1997).
[36]L. Serrano-Andres and M. Fülscher, J. Am. Chem. Soc. **118**, 12190 (1996).
[37]L. Serrano-Andres and M. Fülscher, J. Phys. Chem. B **105**, 9323 (2001).
[38]A. Dongre, J. Jones, A. Somogyi, and V. Wysocki, J. Am. Chem. Soc. **118**, 8365 (1996).
[39]Y. Hu, B. Hadas, M. Davidovitz, B. Balta, and C. Lifshitz, J. Phys. Chem. A **107**, 6507 (2003).
[40]K. Walter, J. Lindner, J. Grotemeyer, and E. Schlag, Chem. Phys. **125**, 155 (1988).
[41]R. Weinkauf, P. Schanen, D. Yang, S. Sonkara, and E. Schlag, J. Phys. Chem. **99**, 11255 (1995).
[42]H. Jochims, M. Schwell, H. Baumgärtel, and S. Leach, Chem. Phys. **314**, 263 (2005).
[43]O. Plekan, V. Feyer, R. Richter, M. Coreno, M. de Simone, K. C. Prince, and V. Carravetta, J. Phys. Chem. A **111**, 10998 (2007).
[44]O. Plekan, V. Feyer, R. Richter, M. Coreno, and K. C. Prince, Mol. Phys. **106**, 1143 (2008), Proceedings of the 20th Colloquium on High Resolution Molecular Spectroscopy, Dijon, France, 3–7 September 2007.
[45]R. Antoine, I. Compagnon, D. Rayane, M. Broyer, P. Dugourd, G. Breaux, F. Hagemeister, D. Pippen, R. Hudgins, and M. Jarrold, J. Am. Chem. Soc. **124**, 6737 (2002).
[46]I. A. Papayannopoulos, Mass Spectrom. Rev. **14**, 49 (1995).
[47]B. Paizs and S. Suhai, Mass Spectrom. Rev. **24**, 508 (2005).